DALTON
FULL PAPER

Crystal structures, electronic properties and structural pathways of thirty [Cu(bipy)$_2$X][Y] complexes, where X = Cl$^-$, Br$^-$ or I$^-$ †

Cathal O'Sullivan, Gillian Murphy, Brian Murphy ‡ and Brian Hathaway *

The Chemistry Department, University College Cork, Ireland. E-mail: stch8001@bureau.ucc.ie

Received 24th December 1998, Accepted 30th March 1999

The crystal structures of ten distortion isomers of the [Cu(bipy)$_2$X]$^+$ cation have been determined, where X = Cl$^-$ (2), Br$^-$ (5) or I$^-$ (3), and compared by scatter plot analysis with twenty [Cu(bipy)$_2$X]Y complexes of known crystal structure. In the ten new structures two involve a near regular trigonal bipyramidal stereochemistry (τ = 0.94–0.90) and eight show a square based pyramidal distorted trigonal bipyramidal stereochemistry (τ = 0.89–0.49), where $\tau = (\alpha_8 - \alpha_1)/60$ [where α_1 = N(2)–Cu–Cl, α_8 = N(1)–Cu–N(3)]. Scatter plots of the eighteen cation distortion isomers of the [Cu(bipy)$_2$Cl][Y] series of complexes suggest that all eighteen complexes lie on a common structural pathway, involving a mixture of the symmetric, C_2, and the asymmetric, non-C_2, in-plane modes of vibration of the CuN$_4$Cl chromophore. The resulting structural pathways are consistent with the direct observation of the effect of the modes of vibration on the stereochemistries of the complexes. A comparison of the trends in the bipy/Cl, Br and I data suggests a size effect of the Br$^-$ and I$^-$ ligands.

Introduction

The role of vibronic coupling[2] in determining the stereochemistry of the copper(II) ion is well documented in the dynamic[3] and pseudo-dynamic[4] Jahn–Teller effect,[5] but is less well documented in establishing their structural pathways.[6] There is an extensive literature on the role of vibronic coupling in determining the structural pathways of the main group inorganic, four-, five- and six-co-ordinate structures,[7] but significantly less on transition metal structures,[8] especially of the copper(II) ion, due to the limited number of data sets available.[9] The five-co-ordinate structural pathways of the [Cu(bipy)$_2$Cl][Y] complexes, Scheme 1, were first reported using five structures,[10] later with nine[11] and now has been increased to eighteen. To obtain this extended data base of thirty complexes, the crystal structures of ten [Cu(bipy)$_2$X]Y complexes, 2Cl$^-$, 5Br$^-$ and 3I$^-$ complexes, have been determined and are now reported.

Results

Fig. 1 shows a representative molecular structure for the [Cu(bipy)$_2$Cl]$^+$ cation, the atom numbering and the angular notation schemes used. Table 1(a) reports[10–21] the Cu–L distances and α_{1-10} angles of the eighteen [Cu(bipy)$_2$Cl][Y] complexes, **1**–**18**. Table 1(b) lists[22,23] the corresponding data for seven [Cu(bipy)$_2$Br]$^+$ cations, **19**–**25**, and Table 1(c) lists[23,24] the data for the five [Cu(bipy)$_2$I]$^+$ cations, **26**–**30**, thus extending the database to thirty [Cu(bipy)$_2$X]$^+$ cations. The corresponding τ values, where $\tau = (\alpha_8 - \alpha_1)/60$,[25] are listed, with τ = 1.00 for a RTBP stereochemistry and τ = 0.00 for a RSBP stereochemistry, where RTBP = regular trigonal bipyramidal,

† Comparative crystallography. Part 6.[1] *Supplementary data available*: preliminary crystal and refinement data for complexes **15**, **27**, and **30**. For direct electronic access see http://www.rsc.org/suppdata/dt/1999/1835/, otherwise available from BLDSC (No. SUP 57534, 2 pp.) or the RSC Library. See Instructions for Authors, 1999, Issue 1 (http://www.rsc.org/dalton).

‡ Present address: Department of Applied Science, Institute of Technology, Sligo, Ireland.

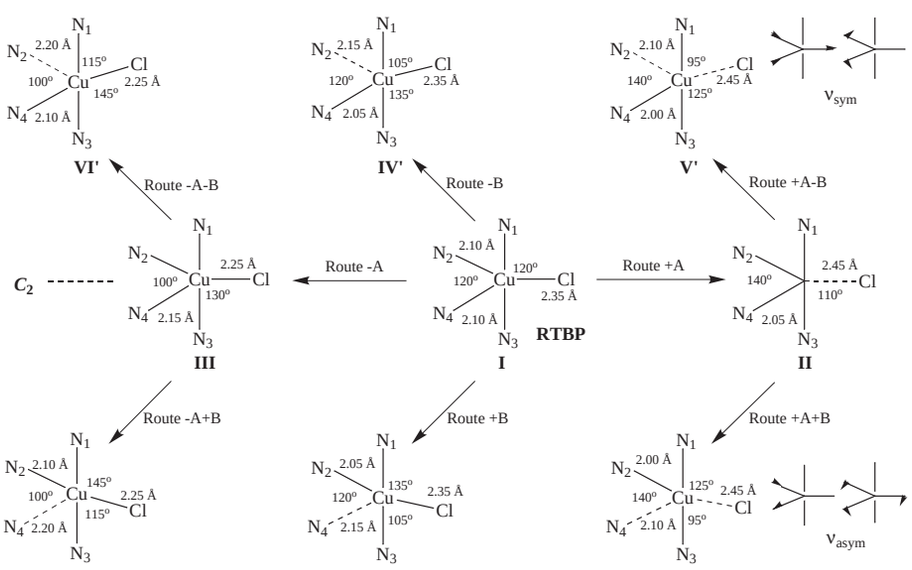

Scheme 1 The forms of distortion of the RTBP CuN$_4$Cl chromophore involving the ±A, ±B and ±A ± B route distortions.

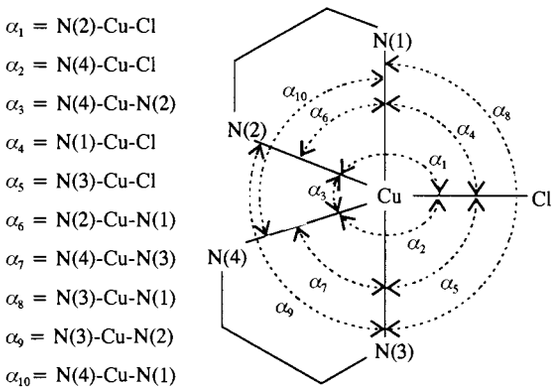

Fig. 1 The atom numbering scheme and a_n notation for the general $[Cu(bipy)_2Cl]^+$ chromophore.

SBPDTBP = square based pyramidal distorted trigonal bipyramidal and RSBP = regular square based pyramidal. Table 2 reports the maximum and minimum values of the Cu–L distances and a_n angles, their differences and average values. Within the near RTBP and SBPDTBP stereochemistries of Table 1 the axial directions, N(1) and N(3), are defined as the largest N–Cu–N angle of *ca.* 180°. The longest in-plane distance, Cu–N(4) is defined as opposite the largest in-plane angle a_1, with $a_1 > a_2 > a_3$. While the observed Cu–Cl distances appear longer than the in-plane Cu–N(2,4) distances, this is only due to the larger covalent radii[26] of the Cl atom relative to the nitrogen atom, *i.e.* 0.99 and 0.70 Å, respectively. If the Cu–Cl distances are corrected for this difference, −0.29 Å, the Cu–N* distances are comparable to the Cu–N(2) distances and less than the Cu–N(4) distances. In Table 1, **9** is the only complex[18] which does obey this requirement as $a_2 < a_1$, but in this complex the Cl ligand bridges to a copper(I) atom and this structure should be considered exceptional. The results for the new structures will not be compared in detail, but compared with the earlier data by scatter plot analysis.

Discussion

For the eighteen $[Cu(bipy)_2Cl][Y]$ complexes, Table 1(a), the structure of the five-co-ordinate CuN_4Cl chromophore varies from near RTBP to intermediate between RTBP and RSBP, *i.e.* SBPDTBP. This is reflected in a range of τ values from 1.00 to 0.53, $\Delta = 0.47$ for a series of five-co-ordinate cation distortion isomers involving the **same** CuN_4X chromophore, with the same set of ligand atoms. Five of the complexes **1**–**5** have τ values in the limited range of 1.00 to 0.94, with a near RTBP stereochemistry, while thirteen, have values in the range 0.79 to 0.53, **6**–**18**, inclusive, and have SBPDTBP stereochemistries. From Table 1(a) it is noticeable that within the range of τ values of 1.00–0.53 there is a significant gap of 0.15 in the lowest τ value of the near RTBP complexes, 0.94 for **5**, and the highest τ value of 0.79 in the group of thirteen. These five near RTBP complexes show only small changes in the Cu–L bond distances and a_n angles, which may be random. Four of the complexes, **1**–**4**, show a_3 angles 1–4° above 120°, varying only 120.7–123.8°, possibly indicative of a small +A route distortion of Scheme 1. The remaining thirteen complexes show significant variations from RTBP, in the −A route distortions of Scheme 1, especially in the three in-plane distances, Cu–Cl, Cu–N(2,4) and angles, a_{1-3}, Table 1(a). In the shift from the near RTBP towards the SBPDTBP stereochemistries, the Cu–N(4) distance, opposite the large a_1 angle, is clearly greater than the Cu–N(2) distance. This suggests that the complexes are largely associated with the −A+B route distortion[10,11] of the RTBP stereochemistry of Scheme 1, but in these bipy/Cl complexes there is a clear absence of the near RSBP stereochemistry, with a τ value of 0.0–0.2.

The bond length and bond angle data for the seven $[Cu(bipy)_2Br]Y$ complexes,[22,23] **19**–**25** inclusive, Table 1(b), show comparable ranges of τ values, 0.91–0.49, while the five $[Cu(bipy)_2I]Y$ complexes,[23,24] **26**–**30**, Table 1(c), show a much more limited range of distortion from the RTBP stereochemistry, τ = 0.89–0.80.

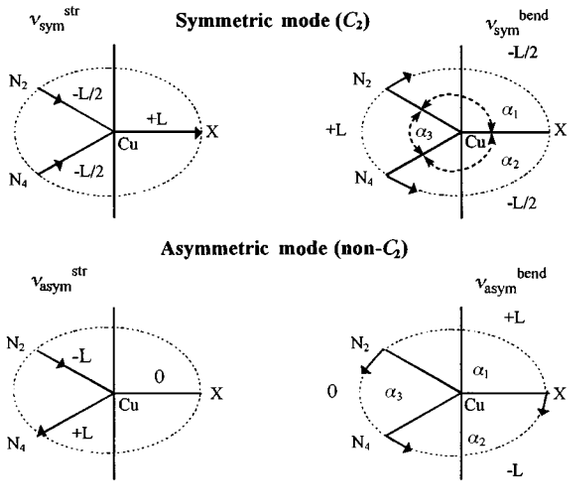

Fig. 2 The symmetric and asymmetric modes of vibration for the five-co-ordinate CuN_4X chromophore, including the relative magnitudes (L).

Table 2 reports the minimum, maximum, ranges and average values of selected bond distances and bond angles for the eighteen $[Cu(bipy)_2Cl]Y$ complexes confirming the exceptional ranges of the Cu–N(4) and Cu–Cl distances and in the a_1 and a_3 angles. The sum of the three in-plane angles, a_{1-3}, 359.9–360.1° is surprisingly constant, while the sum of the distances, Cu–Cl, Cu–N(2) and Cu–N(4), 6.457–6.557 Å, $\Delta = 0.10$ Å, is more variable and differs from the RTBP sum of 6.538 Å. The Cu–N(2,4) distances are constrained by the bite of the chelate ligand, whereas the Cu–Cl distance has no constraint of this type, which may explain why the sum of the in-plane distances does not have an exactly constant value.[1,27,28]

Interpretation of the ±A and ±B route distortions in terms of modes of vibration

The extensive range of the in-plane Cu–L distances and of the a_{1-3} angles for the $[Cu(bipy)_2Cl]Y$ complexes, Table 2, 0.13 Å and 27°, respectively, have only been interpreted in term of the %±A and %±B route distortions[27] of Scheme 1, but it has been suggested[1,10,11,27,28] that these routes may be understood, alternatively, in terms of the in-plane modes of vibration of the CuN_4Cl chromophore,[29–32] Fig. 2. The highest possible symmetry for the CuN_4Cl chromophore is C_2.[29,30] This is restricted to the Cu–Cl direction of the CuN_4Cl chromophore, ±A route, and one that is quite distinct from the two ±B route distortions, which are separately related by an external twofold axis of symmetry. In practice, the CuN_4Cl chromophores display no elements of symmetry, *i.e.* they have C_1 symmetry, Table 1 and Fig. 3. In this symmetry all four in-plane modes of vibration are of A symmetry and can couple into a progression. The observation of a clear linear plot in the a_3 *versus* Cu–Br plot of the $[Cu(phen)_2Br]^+$ cation, Fig. 4(c), ref. 1, is the best evidence for the coupling of the $\nu_{sym}^{bend} + \nu_{sym}^{str}$ modes of vibration in the vibronic coupling model. The observation of clear parallel plots in the same Fig. 4(c)[1] is the best observation of the presence of pure $n\nu_{sym}^{bend}$ and $n\nu_{sym}^{str}$ progressions of the separate modes of vibration. However, as the actual data points rarely involve pure ±A or ±B route distortions, all four modes are generally involved in the distortion of each complex.

Scatter plot analysis of the thirty $[Cu(bipy)_2X][Y]$ complexes

The data for the thirty $[Cu(bipy)_2X][Y]$ complexes, Table 1(a)–(c), are presented in this section, Figs. 4–8, and will be

Table 1 Selected bond lengths (Å) and bond angles (°)

(a) $[Cu(bipy)_2Cl]Y$

Y	$[OH]^-\cdot 6H_2O$	$[PF_6]^-\cdot H_2O$	$Cl^-\cdot 6H_2O$	$[\frac{1}{2}OH^- \cdot \frac{1}{2}Cl^-]$	$[(CH_3)_2C_6H_3SO_3]^-\cdot H_2O$	$[NO_3]^-\cdot 3H_2O$
	1	**2**	**3**	**4**	**5**	**6**
Ref.	12	13	14	15	Present	10
Cu–Cl	2.374(5)	2.344(2)	2.361(4)	2.354(8)	2.337(1)	2.308(3)
Cu–N(1)	1.983(11)	1.996(6)	1.989(10)	1.982(19)	1.982(3)	1.989(6)
Cu–N(2)	2.080(12)	2.105(6)	2.077(10)	2.077(21)	2.093(2)	2.089(6)
Cu–N(3)	1.994(11)	2.005(6)	1.970(10)	2.018(19)	1.988(3)	1.989(6)
Cu–N(4)	2.088(13)	2.108(6)	2.087(10)	2.078(21)	2.101(2)	2.112(5)
a_1	118.7(3)	115.7(2)	118.7(3)	119.0(6)	118.6(1)	127.8(2)
a_2	118.7(4)	120.5(2)	118.6(3)	120.2(6)	121.6(1)	123.4(2)
a_3	122.6(4)	123.8(2)	122.8(4)	120.7(7)	119.8(1)	108.8(2)
a_4	89.7(4)	92.2(2)	90.9(3)	88.8(8)	93.3(1)	93.1(2)
a_5	91.5(4)	92.1(2)	90.9(3)	93.5(7)	91.9(1)	92.0(2)
a_6	80.2(5)	79.6(2)	79.3(4)	80.2(8)	80.2(1)	79.9(3)
a_7	80.1(5)	80.1(2)	79.8(4)	78.1(7)	80.4(1)	80.2(2)
a_8	178.7(5)	175.5(2)	178.3(4)	177.2(9)	174.7(1)	174.9(2)
a_9	99.6(5)	99.8(2)	100.0(4)	99.3(8)	96.1(1)	96.6(2)
a_{10}	98.9(5)	96.4(2)	99.3(5)	100.2(2)	98.1(1)	97.6(2)
τ	1.00	1.00	0.99	0.97	0.94	0.79

Y	$\frac{1}{2}[S_5O_6]^-\cdot 6H_2O$	$[CuCl_2]^-\cdot C_6O_6H_4$	$[CuCl_2]^-$	$[BF_4]^-$	$[CF_3SO_3]^-\cdot H_2O$(I)	$[MoS_4Cu_2Cl_3]$
	7	**8**	**9**	**10**	**11**	**12**
Ref.	16	17	18	11	Present	19
Cu–Cl	2.292(4)	2.294(1)	2.356	2.285(3)	2.259(1)	2.273(3)
Cu–N(1)	1.992(6)	1.991(3)	1.985	2.006(7)	1.986(5)	1.981(8)
Cu–N(2)	2.092(6)	2.071(3)	2.063	2.079(8)	2.091(4)	2.076(8)
Cu–N(3)	1.988(6)	1.988(3)	1.995	1.983(7)	1.973(4)	1.978(8)
Cu–N(4)	2.106(5)	2.104(3)	2.086	2.142(8)	2.128(3)	2.124(8)
a_1	130.7(1)	131.7(1)	133.4	134.8(3)	133.1(1)	134.0(2)
a_2	122.0(2)	121.1(1)	111.1	127.6(3)	119.9(1)	119.8(2)
a_3	107.3(2)	107.1(1)	115.5	97.6(3)	106.9(1)	106.2(2)
a_4	92.0(2)	92.71(9)	91.0	93.1(3)	93.9(1)	93.5(2)
a_5	93.3(2)	91.88(9)	93.5	91.7(3)	92.8(1)	94.7(2)
a_6	79.9(3)	79.8(1)	80.0	79.9(3)	79.8(2)	80.0(3)
a_7	79.7(2)	79.6(1)	80.2	79.5(3)	79.9(2)	79.8(4)
a_8	174.8(2)	174.7(1)	175.3	175.2(4)	173.2(2)	171.8(3)
a_9	96.7(3)	95.2(1)	97.0	97.8(3)	96.9(2)	95.2(3)
a_{10}	97.5(2)	100.2(1)	97.0	96.7(3)	95.4(2)	95.0(3)
τ	0.74	0.72	0.70	0.67	0.67	0.63

Y	$[ClO_4]^-$	$[WS_4Cu_2Cl_3]^-$	$[CF_3(CF_2)_3SO_3]^-$	$[(NC)_5C_2]^-$	$[(CN)_4(quin)]^-$	$[CF_3SO_3]^-\cdot H_2O$ (II)
	13	**14**	**15**	**16**	**17**	**18**
Ref.	10	19	[a]	20	21	Present
Cu–Cl	2.263(3)	2.275(3)	2.284(2)	2.277(3)	2.301	2.246(2)
Cu–N(1)	1.993(4)	1.979(8)	1.993(6)	1.969(8)	1.990	1.981(4)
Cu–N(2)	2.076(3)	2.071(8)	2.061(6)	2.062(9)	2.066	2.083(4)
Cu–N(3)	1.991(4)	1.973(8)	1.969(6)	1.998(8)	1.904	1.995(4)
Cu–N(4)	2.136(5)	2.139(8)	2.140(6)	2.118(8)	2.126	2.140(4)
a_1	137.1(1)	136.2(2)	136.8(2)	138.5(2)	135.6	140.4(1)
a_2	126.4(2)	121.1(2)	119.2(2)	114.2(2)	116.0	119.1(1)
a_3	96.5(2)	102.6(3)	104.0(2)	107.3(3)	108.4	100.6(1)
a_4	93.4(2)	93.9(3)	93.9(2)	93.6(2)	94.0	95.1(1)
a_5	92.1(2)	92.1(3)	92.1(2)	92.0(2)	94.5	92.5(1)
a_6	80.1(2)	80.6(3)	79.8(3)	80.3(3)	79.9	79.7(2)
a_7	79.2(2)	79.5(4)	79.5(2)	78.6(3)	80.8	79.2(2)
a_8	174.5(1)	173.6(4)	173.9(3)	174.3(3)	171.3	172.2(2)
a_9	96.0(2)	95.6(2)	96.5(2)	96.4(3)	92.6	95.8(2)
a_{10}	97.4(2)	96.5(3)	96.5(3)	97.9(3)	98.4	95.3(2)
τ	0.62	0.62	0.62	0.60	0.60	0.53

(b) $[Cu(bipy)_2Br]Y$

Y	$[PF_6]^-\cdot H_2O$	$[NO_3]^-\cdot H_2O$	$[ClO_4]^-$	Br^-	$[BF_4]^-$	$[BPh_4]^-$	$[CF_3SO_3]^-\cdot H_2O$
	19	**20**	**21**	**22**	**23**	**24**	**25**
Ref.	Present	Present	Present	22	23	Present	Present
Cu–Cl	2.469(1)	2.514(1)	2.466(1)	2.429(2)	2.419(3)	2.419(1)	2.418.(1)
Cu–N(1)	1.991(3)	1.982(4)	1.986(3)	1.977(6)	1.996(7)	1.984(2)	1.997(4)
Cu–N(2)	2.093(3)	2.082(4)	2.094(3)	2.075(8)	2.068(8)	2.105(3)	2.067(4)
Cu–N(3)	1.990(3)	1.991(4)	1.999(3)	1.978(6)	1.995(7)	1.981(2)	2.002(4)
Cu–N(4)	2.096(3)	2.089(4)	2.098(3)	2.085(7)	2.114(9)	2.131(3)	2.169(5)

Table 1 (*contd.*)

(b) (*contd.*)

Y	$[PF_6]^-\cdot H_2O$ **19**	$[NO_3]^-\cdot H_2O$ **20**	$[ClO_4]^-$ **21**	Br^- **22**	$[BF_4]^-$ **23**	$[BPh_4]^-$ **24**	$[CF_3SO_3]^-\cdot H_2O$ **25**
Ref.	Present	Present	Present	22	23	Present	Present
a_1	120.9(1)	123.9(1)	123.5(1)	128.6(2)	134.5(2)	136.6(1)	140.3(1)
a_2	122.4(1)	116.1(1)	123.1(1)	124.7(2)	126.2(3)	124.7(1)	113.1(1)
a_3	116.6(1)	120.1(1)	113.4(1)	106.7(3)	99.4(3)	98.6(1)	106.6(2)
a_4	91.6(1)	92.4(1)	93.3(1)	90.4(2)	93.0(3)	94.8(1)	96.2(1)
a_5	92.9(1)	90.5(1)	91.7(1)	91.4(2)	91.2(3)	93.8(1)	93.4(1)
a_6	80.4(1)	80.0(2)	79.8(1)	80.4(3)	80.1(3)	79.7(1)	80.3(2)
a_7	79.8(1)	79.4(2)	79.7(1)	80.3(3)	79.6(3)	79.3(1)	79.2(2)
a_8	175.2(1)	177.1(2)	174.7(1)	177.3(3)	175.6(2)	171.3(1)	169.7(2)
a_9	95.9(1)	98.5(2)	98.9(1)	96.9(3)	97.7(3)	93.7(1)	94.7(2)
a_{10}	99.2(1)	99.2(2)	96.0(1)	100.3(3)	97.0(3)	96.0(1)	93.5(2)
τ	0.91	0.89	0.85	0.81	0.69	0.58	0.49

(c) $[Cu(bipy)_2I]Y$ **26–30**, $[Cu(phen)_2X]Y$ (X = Cl **31** or Br **32**)

Y	I^- —	$[PF_6]^-$ **26**	I^- **27**	$[ClO_4]^-$ **28**	$[BPh_4]^-$ **29**	$[CF_3SO_3]^-\cdot H_2O$ **30**	$[BPh_4]^-$ **31**	$[BPh_4]^-$ **32**
Ref.	24	Present	[a]	23	Present	[a]	27	1
Cu–I	2.70(4)	2.688(1)	2.677(1)	2.675(4)	2.676(1)	2.676(1)	2.254(1)	2.398(1)
Cu–N(1)	2.00(4)	1.993(4)	1.992(4)	1.989(6)	1.989(3)	1.990(5)	2.024(2)	2.025(3)
Cu–N(2)	1.96(4)	2.084(4)	2.083(4)	2.090(8)	2.103(3)	2.096(5)	2.057(2)	2.055(3)
Cu–N(3)	2.03(4)	1.990(4)	1.978(4)	1.987(6)	2.000(3)	1.989(5)	2.008(2)	1.997(3)
Cu–N(4)	2.10(4)	2.090(4)	2.084(4)	2.100(7)	2.103(3)	2.107(6)	2.242(2)	2.217(3)
a_1	121(2)	121.3(1)	122.9(1)	122.9(2)	127.6(1)	123.3(1)	157.7(1)	157.2(1)
a_2	124(2)	121.2(1)	123.0(1)	122.8(2)	120.3(1)	121.2(1)	105.9(1)	105.9(1)
a_3	113(2)	117.4(1)	114.1(2)	114.3(3)	112.2(1)	115.5(2)	96.4(1)	96.8(1)
a_4	89(2)	91.4(1)	90.1(1)	93.8(2)	92.3(1)	92.0(1)	92.7(1)	93.3(1)
a_5	91(2)	93.6(1)	94.2(1)	91.0(2)	92.1(1)	93.7(1)	91.4(1)	91.0(1)
a_6	81(2)	80.4(1)	80.2(2)	80.3(3)	79.8(1)	80.3(2)	81.0(1)	81.2(1)
a_7	83(2)	80.0(2)	79.9(2)	80.1(1)	80.1(1)	80.0(2)	79.2(1)	79.8(1)
a_8	175(2)	174.7(1)	174.6(2)	174.4(2)	175.5(1)	174.1(1)	169.2(1)	170.2(1)
a_9	95(2)	95.4(2)	100.2(2)	99.5(3)	98.0(1)	95.2(2)	91.5(1)	91.5(1)
a_{10}	99(2)	98.9(2)	94.9(2)	94.9(3)	97.0(1)	98.4(2)	109.1(1)	107.4(1)
τ	0.90	0.89	0.86	0.86	0.80	0.85	0.19	0.22

[a] Preliminary data, see SUP 57534.

Table 2 The minima, maxima, ranges and averages of selected bond lengths (Å) and angles (°) for the $[Cu(bipy)_2Cl]Y$ series **1–18**

	Out-of-plane bond lengths		In-plane bond lengths		
	Cu–N(1)	Cu–N(3)	Cu–N(2)	Cu–N(4)	Cu–Cl
Minimum	1.969(8)	1.904(6)	2.061(6)	2.078(2)	2.246(2)
Maximum	2.006(7)	2.018(2)	2.105(6)	2.142(8)	2.374(5)
Range	0.037	0.114	0.044	0.064	0.128
Average	1.987	1.983	2.078	2.115	2.305

	In-plane angles			Out-of-plane angles						
	a_1	a_2	a_3	a_4	a_5	a_6	a_7	a_8	a_9	a_{10}
Minimum	115.7(2)	111.1	96.5(2)	88.8(8)	90.9(3)	79.3(4)	78.1(7)	171.3(2)	92.6(2)	95.0(3)
Maximum	140.4(1)	127.6	123.8(2)	95.1(1)	94.7(2)	80.6(3)	80.8(3)	178.7(5)	100.0(4)	100.2(4)
Range	24.7	16.5	27.3	6.3	3.8	1.3	2.7	7.4	7.4	5.2
Average	130.0	120.0	109.9	92.7	92.5	80.0	79.7	174.7	96.8	97.5

Average Cu–N(1,3) = 1.985 Å (out of plane), average Cu–N(2,4) = 2.097 Å (in-plane).

compared using scatter plot analysis. Initially, the data for the eighteen bipy/Cl complexes will be discussed and subsequently the bipy/Br and bipy/I data will be briefly considered. A general discussion of the use of scatter plots has been reported previously[27] and will now be applied to the thirty $[Cu(bipy)_2X]^+$ cations. Using the suggested limiting values[27,28] for the ±A, ±B and ±A±B route distortions illustrated in Scheme 1, the angle *versus* angle plots and the distance *versus* distance plots can be divided up to represent ±A, ±B axes and ±A±B sections, Figs. 4–8. In order to compare the Cu–X distances, the observed Cu–Br and Cu–I distances are corrected[26] to the corresponding Cu–Cl* distances by subtracting the difference in the covalent radii, Cu–Br, −0.14 Å, and Cu–I, −0.33 Å, respectively. General trends will be discussed, along with the interpretation in terms of the corresponding modes of vibration. From Table 1, the estimated standard deviations (e.s.d.s) of the bond distances using a 3σ criterion are <0.02 Å, giving a spread of ±0.01 Å, and for the bond angles is <2°, giving a spread of ±1°.

The eighteen data points in Fig. 4 vary from RTBP to SBP-

E″	d_{yz}, d_{xz}	B_2, B_1	B B	A A	
E′	d_{xy}, $d_{x^2-y^2}$	B_2, B_1	A_2 A_1	A A	A A
A_1'	d_{z^2}	A_1	A_1	A	A
Symmetry		D_{3h}	C_{4v}	C_{2v}	C_2	C_1
Jahn-Teller Active		No	No	No	No	No
pseudo J. T.	ν_{sym} (C_2)	Yes	No	Yes	Yes	Yes
Active	ν_{asym} (non-C_2)	No	No	No	No	Yes

Fig. 3 The one-electron orbital levels of the RTBP stereochemistry and their symmetries in various point groups.

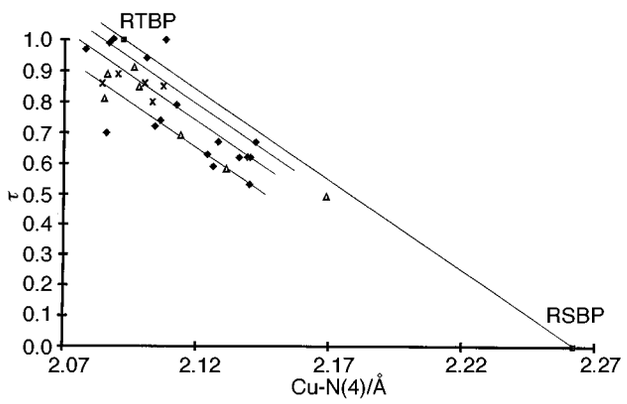

Fig. 4 Plots of τ *versus* Cu–N(4): ◆ bipy/Cl, ■ RTBP, ▲ bipy/Br, × bipy/I.

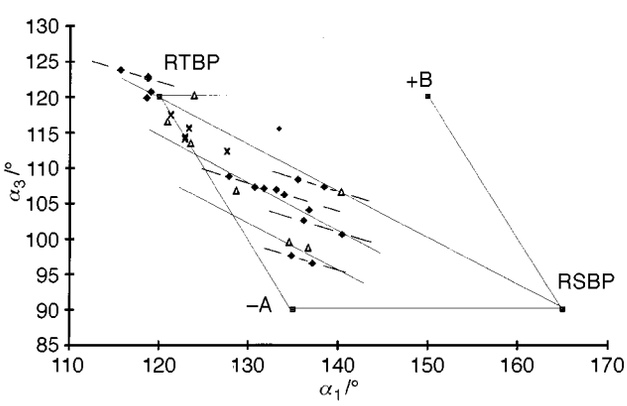

Fig. 5 Plots of a_3 *versus* a_1. Key as in Fig. 4.

DTBP, with the τ values decreasing from 1.00 to 0.53, as the Cu–N(4) distances increase from 2.078 to 2.142 Å, respectively, but with a slight gap in the τ range from 0.91 to 0.79. This suggests a non-continuous structural pathway in the bipy/Cl data points, except that the gap is not filled in the Cu–N(4) distance and is filled by the bipy/Br and I data points. This plot provides a qualitative indication of the range of the observed stereochemistries of the $[Cu(bipy)_2Cl][Y]$ series of complexes. Three possible parallel pathways pass through or close to five, six and three data points, respectively, while one of the remaining data points lies above the RTBP ⟶ RSBP pathway and two lie clearly below the three parallel pathways. The seven bipy/Br data points clearly overlap the bipy/Cl data points, but are shifted to slightly lower τ and Cu–N(4) values. The highest τ value is 0.91 and a single bipy/Br data point involves the lowest τ value 0.49, and highest Cu–N(4) value, 2.169 Å. In contrast, the five bipy/I data points show a much more limited range, with τ ranging from 0.89 to 0.80 and Cu–N(4) distances ranging from 2.107 to 2.084 Å.

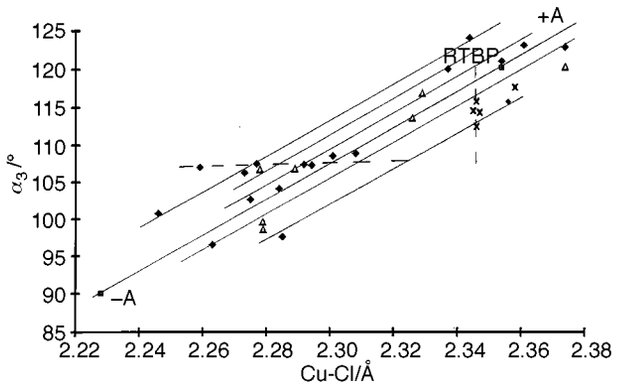

Fig. 6 Plots of a_3 *versus* Cu–Cl. Key as in Fig. 4.

The a_3 values in Fig. 5 decrease from 123.8(2) to 96.5(2)° as the a_1 values increase from 115.7(2) to 140.4(1)°. The eighteen bipy/Cl data points lie in two different sections, the five near RTBP data points lie close to the RTBP data point,[1,27] with a small +A−B route sense of distortion. Four of the bipy/Cl data points display a_3 values slightly above 120° and a_1 angles slightly below 120°, consistent with a small +A route distortion. The remaining thirteen bipy/Cl data points lie in the body of the plot with a substantial −A+B sense of distortion and show an *inverse* trend through the RTBP data point. Two data points lie near the RTBP ⟶ RSBP (−A+B) pathway or its extension, with eight data points lying on or near a clearly parallel pathway (—). Two data points lie on a lower parallel pathway. However, a better correlation of all the bipy/Cl data points is obtained with a series of parallel pathways (– – –), involving a less acute inverse slope, that are not parallel to the RTBP to (– A+B) route and involve a vertical separation of a pure progression of $n\nu_{sym}^{bend}$ modes of vibration. See the discussion of Fig. 8. Two of the bipy/Cl data points lie close to the RTBP ⟶ +A route distortion, but again with the absence of a clear crystallographic twofold axis of symmetry.

The seven bipy/Br data points clearly overlap the bipy/Cl data points and consolidate the occurrence of parallel trend lines. The five bipy/I data points cluster below the RTBP data point. Three of the bipy/I data points lie near the RTBP ⟶ −A route pathway, with near C_2 symmetry, but with only a small displacement from the RTBP stereochemistry. The addition of the seven bipy/Br and five bipy/I data points only marginally improves the (– – –) correlations. None of the thirty bipy/X complexes involves a true crystallographic twofold axis of symmetry, associated with the RTBP ⟶ −A route pathway.

The eighteen bipy/Cl data points of Fig. 6 show a *normal* trend, with the a_3 angles decreasing from 123.8(2) to 96.5(2)°, $\Delta = 27.3°$, as the Cu–Cl distances decrease from 2.374(5) to 2.246(2) Å, $\Delta = 0.128$ Å. Three data points lie on the central +A ⟶ RTBP ⟶ −A correlation. Five data points lie on a higher parallel correlation, four on an even better higher correlation and two sets of two, on two lower correlations. The graph can be again divided into two sections, +A, where $a_3 > 120°$ and Cu–Cl > 2.354 Å, and −A, where $a_3 < 120°$ and Cu–Cl < 2.354 Å. However, in the +A extension, for four data points, the deviation from RTBP is only small, $\Delta a_3 = 3.8°$, relative to the −A extension data points, where $\Delta a_3 = 23.5°$. Consequently, the $[Cu(bipy)_2Cl][Y]$ complexes involve a predominantly −A route distortion. As the a_3 angle and the Cu–Cl distance involve the pure ν_{sym}^{bend} and ν_{sym}^{str} modes of vibration, respectively, the plot of Fig. 6 represents a further example[1,27] of linear and parallel coupling of these modes of vibration of A symmetry. The observation of four data points with a virtually horizontal correlation (– – –) is an example of a horizontal progression of a pure $n\nu_{sym}^{str}$ (−A route distortion) mode of vibration at a constant a_3 angle of 107°.

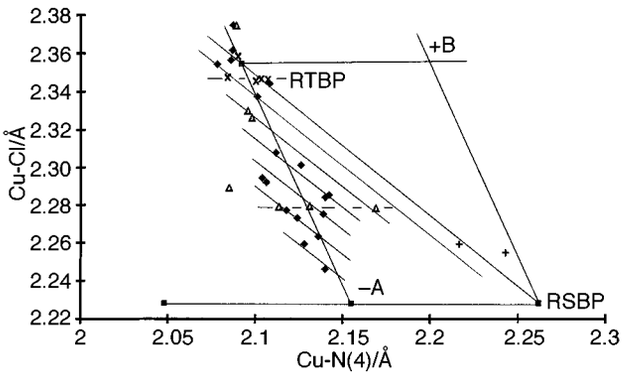

Fig. 7 Plots of Cu–Cl *versus* Cu–N(4). Key as in Fig. 4, + phen/Cl, Br.

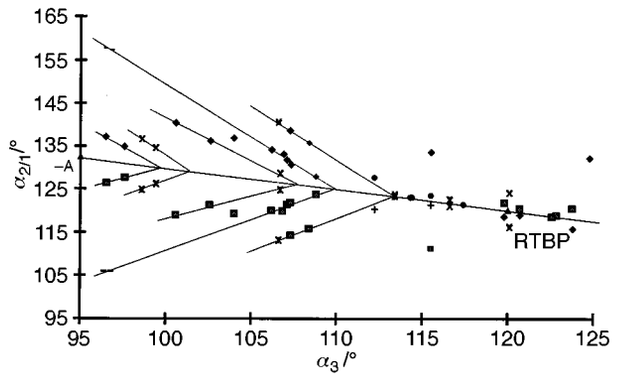

Fig. 8 Plots of $a_{2/1}$ *versus* a_3: ◆ bipy/Cl-1, ■ bipy/Cl-2, ▲ RTBP, × bipy/Br-1, * bipy/Br-2, ● bipy/I-1, + bipy/I-2, − phen/Cl-1, — phen/Cl-2

The seven bipy/Br data points, with corrected Cu–Cl* distances, 2.278–2.374 Å, overlap the bipy/Cl data points. The points do not extend the ranges of the a_3 angle or the corrected Cu–Cl* distance, but they do consolidate the linear and parallel correlations. The five bipy/I data points cluster in the much more limited range of a_3 of 112.2–117.4° and the corrected Cu–Cl* distance of 2.345–2.358 Å. They only contribute to the linear and parallel correlations just below the near RTBP data point, but four of the bipy/I data points display a clear vertical progression consistent with a pure nv_{sym}^{bend} (−A route distortion) mode of vibration at a constant corrected Cu–Cl* distance of 2.345 Å. In the eighteen bipy/Cl data points of Fig. 6 there is a clear separation of the six near RTBP and twelve SBPDTBP data points, a gap that is spanned by two of the bipy/Br and three of the bipy/I data points.

The eighteen bipy/Cl data points in Fig. 7 range from 2.246 to 2.374 Å in the Cu–Cl distance and from 2.078 to 2.142 Å in the Cu–N(4) distance, with a slight gap in the Cu–Cl data points from 2.31 to 2.34 Å, but not in the Cu–N(4) distance. There are six data points clustering about the RTBP data point, possibly with a random distribution. The remaining twelve data points are spread about the RTBP ⟶ −A route distortion, with a 35–85% extension along the −A route and ±20% ±B, with an *inverse* correlation. Correlations may be drawn in the bipy/Cl data parallel to the RTBP ⟶ RSBP pathway, through four, three, two and one data points, but these are significantly displaced from the main pathway. This displacement is most noticeable at the lower Cu–Cl distances, suggesting that the Cu–N(4) distances are more associated with the RTBP ⟶ −A route pathway of the "see-saw", Type III structure[28] of Scheme 1. The displacement of the Cu–N(4) distances to lower values, can be understood in terms of a horizontal flip through a progression of pure nv_{asym}^{str} modes of vibration, giving a false association of the Cu–N(4) distances with the RTBP ⟶ −A route distortion. Three of the bipy/Cl data points show a good linear correlation along the RTBP ⟶ −A route, but as in none of these cases are the Cu–N(2) and Cu–N(4) distances equal, the correlation is an artefact of the shift to lower Cu–N(4) distances with the decreasing Cu–Cl distances discussed above.

The seven bipy/Br data points, with corrected Cu–Cl* distances, largely overlap the bipy/Cl data points and only extend the range of the Cu–N(4) distances, slightly, to 2.17 Å. The bipy/Cl Cu–Cl gap is bridged by two of the bipy/Br data points. They consolidate the linear and parallel correlations and the displacement of the Cu–N(4) distances to lower values. Three of the bipy/Br data points display a horizontal correlation at a constant Cu–Cl* distance of 2.28 Å, suggesting a pure nv_{asym}^{str} progression contribution to the Cu–N(4) distance. The five bipy/I data points cluster in the much more limited range of the Cu–Cl* distance of 2.345–2.358 Å and of the Cu–N(4) distance of 2.084–2.107 Å and they only contribute to the linear and parallel correlations just below the near RTBP data point. Four of the bipy/I data points display a clear horizontal progression consistent with a pure nv_{asym}^{str} progression contribution to the Cu–N(4) distance at a constant Cu–Cl* distance of 2.345 Å. These two horizontal correlations in the bipy/Br and bipy/I data points suggest that the Cu–Cl* distances are limited by the larger size of the Br^- and I^- anions, relative to that of the Cl^- anion, that limits the effect of the v_{sym}^{str} mode of vibration.

For the bipy/Cl data, the plot of $a_{2/1}$ *versus* a_3 in Fig. 8 involves $a_{2/1}$ angles ranging from 140 to 110° and a_3 angles from 124 to 96° and indicates a general increase in the separate a_2 and a_1 angles from high to low a_3 angles. At high a_3 angles, 124–119°, the spread in $\Delta a_{2/1}$ is small, 5°, as $a_1 + a_2 + a_3 = 360°$, but at lower a_3 angles, 116–102°, the spread increases to a maximum of 27° at 107° and then decreases to 8° at a_3 angles of 100–96°. The average $a_{1,2}$ angle of 120° at an a_3 angle of 120° increases to 132.5° (−A route) at an a_3 angle of 95° and corresponds to the effect of the pure v_{sym}^{bend} on the a_3 angle. Within the a_3 range of 120–95°, the values of the individual a_1 and a_2 angles are evenly spread about the mean $a_{1,2}$ line. This corresponds to the effect of a pure v_{asym}^{str} mode of vibration superimposed onto the pure v_{sym}^{str} mode of vibration. The symmetric nature of the data of Fig. 8 about the RTBP ⟶ −A route data line and the restriction to the $\Delta a_{1,2}$ angle at high and low a_3 angles suggests a strong link of the $-v_{sym}^{bend}$ and the v_{asym}^{bend} modes of vibration. At the low a_3 angles this is also consistent with the formation of a pure −A route distortion, see-saw structure,[28] where the effect of the v_{asym}^{bend} is reduced to zero. In the see-saw structure $a_1 = a_2 = 135°$ and $a_3 \approx 90°$, as described in ref. 28.

A feature of Fig. 8 is the formation of number of interpenetrating right-pointing arrowhead structures, generated by reasonably linear correlations of the separate a_1 and a_2 data points against the a_3 data points. For this purpose the data for structure **9** are treated as exceptional, see earlier. Within each arrowhead the spread in the $\Delta a_{2,1}$ angles and the range in the a_3 angles are limited to <27 and 7°, respectively, and the tip of the arrow lies on the RTBP ⟶ −A route pathway. This suggests that as a_3 decreases there is a limit to the spread in $\Delta a_{2,1}$ and the a_3 angle flips to a lower value. Thus, Fig. 8 presents a clear visual picture of the combined effect of the v_{sym}^{bend} and the v_{asym}^{bend} modes of vibration on the in-plane a_{1-3} angles.

In Fig. 5 two sets of parallel correlations were suggested, the first set (—) parallel to the RTBP ⟶ RSBP pathway and the second set (– – –), with a more acute inverse correlation. This second set corresponds with the right pointing arrowhead structures of Fig. 8. Each arrowhead then corresponds to a separate parallel pathway of Fig. 5 and to a limited range of a_3 angles.

If the corrected bipy/Br data points are added to Fig. 8 they endorse the shorter right pointing arrowhead structures, by adding to the existing arrows or by generating a separate arrowhead. The five bipy/I data points are significantly different in that the a_3 angles are all in the range 118–112° and the $\Delta a_{2/1}$ angles are less than 7°. However, three of the data points are

very close to a crystallographic twofold axis and could represent the tip of an arrowhead, if more data were available. Together, the thirty bipy/X data points provide even more convincing evidence of the right-pointing arrowhead sub-structure and for the suggestion of the ranges of the a_3 angles of Fig. 8, that is also supported by the alternative parallel pathways of Fig. 5.

General conclusions from the bipy/X scatter plot data

(a) The data refer to a total of thirty bipy/X single crystal structures of the same $[Cu(bipy)_2X]^+$ cation distortion isomers, where $X = Cl^-$ (18), Br^- (7) and I^- (5), in lattices of different $[Y]^-$ anions.

(b) The stereochemistry of the CuN_4Cl chromophores range from six near RTBP, $\tau \approx 1.0$, to twelve SBPDTBP, with τ ranging from 0.79 to 0.53, the seven CuN_4Br chromophores range from 0.91 to 0.49 and the five CuN_4I chromophores range from τ 0.89 to 0.80. These ranges are associated with a variation of the crystal environment of each $[Cu(bipy)_2X]^+$ cation, associated with the different Y^- anions present.

(c) Of the eighteen bipy/Cl data points, five cluster about the RTBP data point, in possibly a random distribution, $\tau = 1.0$–0.94. For the remaining thirteen data points, the distribution is not random and there is clear evidence of linear pathways,[1] largely parallel to the RTBP ⟶ RSBP (−A+B) route distortions associated with the structural pathways of Scheme 1.

(d) Within the three scatter plots of Figs. 5–7, significant linear and parallel correlations are observed, plus some limited horizontal and vertical correlations.[1,27,28] All four types of correlation can be understood in terms of the coupling into linear progressions[28] of the four in-plane modes of vibration of the CuN_4X chromophore,[29,30] all of which are of A symmetry[31,32] in the C_1 point group, Fig. 3.

(e) The existence of six lower pathways parallel to the RTBP ⟶ RSBP (−A+B) route distortion of Fig. 7 accounts for the low numerical values of the Cu–N(4) distances, by vertical "flips" to lower pathways by progressions of $-n\nu_{sym}^{str}$ modes of vibration, in the bulk of the bipy/Cl and bipy/Br data points.

(f) The existence of distinct horizontal sequences in the bipy/Br and bipy/I data points of Fig. 7 is also some evidence for the flips to lower parallel pathways, possibly associated with the increasing size of the co-ordinated anions, $Cl^- < Br^- < I^-$.

(g) Within the scatter plot of Fig. 8, there is clear evidence for a right-pointing arrowhead structure, within which there are limited ranges of a_3 angles. The "flips" to adjacent arrowheads are associated with progressions in the pure $n\nu_{sym}^{str}$ modes of vibration and are related to the individual parallel pathways of Fig. 5.

(h) Together, the scatter plots of Figs. 4–8 present the most convincing evidence for the involvement of the four in-plane modes of vibration of the CuN_4X chromophore, Fig. 2, in determining the directions of distortion along the ±A±B routes of the structural pathways of Scheme 1.

$[Cu(phen)_2X][Y]$ Complexes, $X = Cl^-$, Br^- or I^-

The corresponding series of $[Cu(phen)_2X][Y]$ complexes have been reported previously,[1,27,28] in general there is a close similarity between the phen/X and the present bipy/X complexes, except in one respect. One phen/Cl and one phen/Br complex, both with the $[BPh_4]^-$ anion, Table 1(c), **31** and **32**, have exceptionally low τ values of 0.19 and 0.22, respectively, corresponding with a near RSBP stereochemistry. These data points have been added to Figs. 7 and 8 and justify some comment. In Fig. 7 they are associated with exceptionally long Cu–N(4) distances, for comparable Cu–Cl* distances, associated with the RSBP(−A+B) route distortion. Neither complex is associated with the RTBP ⟶ −A route distortion, or with the "flip" to lower parallel pathways of the bipy/X data points. In Fig. 8 the two phen/X data points are associated with low a_3 angles of 96° and exceptionally large $\Delta a_{2,1}$ angles of ≈50°, clearly different from any of the bipy/X data points. These differences must be associated with the differences in the phen and bipy ligands, as all other factors are equal. Why this difference occurs is not understood, but may be associated with the differing rigidity of the phen and bipy ligands.

Implications

The eighteen $[Cu(bipy)_2Cl]Y$ data points represent the best evidence for the involvement of the modes of vibration of the CuN_4Cl chromophore to account for the wide range of stereochemistry displayed by the same $[Cu(bipy)_2Cl]^+$ cation, from near RTBP, $\tau = 1.00$, to SBPDTBP, $\tau = 0.53$. The independent low temperature structures,[33] at 150 K, of **2** and **31,** not only confirm the original structure determinations,[11,13] but establish the static nature of these extreme stereochemistries[34,35] and confirm the absence of disorder in these cations, thus ruling out the possibility of a pseudo-dynamic[3] or dynamic[4] Jahn–Teller Effect.[5]

A number of accounts[36–38] have been given previously to describe the range of static geometries of the five-co-ordinate

Table 3 Electronic reflectance data for $[Cu(bipy)_2Cl]Y$ complexes

Complex	Y	τ	Peak energy/10^3 cm^{-1}
2	$[Pf_6]^-\cdot H_2O$	1.00	12.00
3	$Cl^-\cdot 6H_2O$	0.99	12.50
4	$[½OH^-, ½Cl^-]$	0.97	12.00
5	$[(CH_3)_2C_6H_3SO_3]^-$	0.94	11.72
6	$[NO_3]^-\cdot 3H_2O$	0.79	13.50(sh), 11.50
7	$½[S_5O_6]-\cdot 6H_2O$	0.74	13.24, 10.47
9	$[CuCl_2]^-$	0.70	12.50
10	$[BF_4]^-$	0.67	13.90, 10.10
11	$[CF_3SO_3]^-\cdot H_2O$	0.67	12.80, 11.17
13	$[ClO_4]^-$	0.62	14.16, 10.10
15	$[CF_3(CF_2)_3SO_3]^-$	0.62	13.42, 10.30

Table 4 The colour and analytical data for the ten new $[Cu(bipy)_2X]Y$ complexes

		Analysis: Found(Calculated) (%)			
Complex	Colour	C	H	N	Cu
5 $[Cu(bipy)_2Cl][(CH_3)_2C_6H_3SO_3]\cdot H_2O$	Blue	54.9(54.7)	4.54(4.43)	9.28(9.12)	10.51(10.34)
11, **18** $[Cu(bipy)_2Cl][CF_3SO_3]\cdot H_2O$	Blue	44.3(44.3)	2.29(3.01)	9.78(9.84)	11.05(11.16)
19 $[Cu(bipy)_2Br][PF_6]\cdot H_2O$	Green	39.9(40.0)	2.56(2.68)	9.24(9.33)	10.82(10.58)
20 $[Cu(bipy)_2Br][NO_3]\cdot H_2O$	Green	45.3(44.8)	3.12(3.39)	13.31(13.07)	11.43(11.86)
21 $[Cu(bipy)_2Br][ClO_4]$	Green	43.7(43.3)	2.84(2.90)	10.10(10.09)	11.14(11.44)
24 $[Cu(bipy)_2Br][BPh_4]$	Green	67.7(68.2)	4.67(4.68)	7.17(7.23)	8.17(8.20)
25 $[Cu(bipy)_2Br][CF_3SO_3]\cdot H_2O$	Green	41.5(41.7)	2.66(2.67)	9.13(9.26)	10.58(10.50)
27 $[Cu(bipy)_2I]I$	Green	38.4(38.2)	2.64(2.56)	8.40(8.90)	10.45(10.09)
29 $[Cu(bipy)_2I][BPh_4]$	Green	64.5(64.3)	4.41(4.41)	6.85(6.82)	7.48(7.73)
26 $[Cu(bipy)_2I][PF_6]$	Green	37.2(37.1)	2.58(2.49)	8.74(8.69)	9.38(9.81)

Table 5 Crystal and refinement data for ten $[Cu(bipy)_2X]Y$ complexes

	5	**11**, **18**	**19**	**20**	**21**	**24**	**25**	**26**	**29**
Chemical formula	$C_{28}H_{27}ClCuN_4O_4S$	$C_{42}H_{34}Cl_2Cu_2F_6N_8O_7S_2$	$C_{20}H_{16}BrCuF_6N_4P$	$C_{20}H_{18}BrCuN_5O_4$	$C_{20}H_{16}BrClCuN_4O_4$	$C_{44}H_{36}BBrCuN_4$	$C_{21}H_{18}BrCuF_3N_4O_4S$	$C_{20}H_{16}CuF_6IN_4P$	$C_{44}H_{36}BCuIN_4$
Formula weight	614.605	1138.865	600.775	535.844	555.274	775.060	622.900	647.770	822.055
Crystal system	Monoclinic	Triclinic	Triclinic	Triclinic	Triclinic	Triclinic	Monoclinic	Triclinic	Monoclinic
Space group	$P2_1/c$	$P\bar{1}$	$P\bar{1}$	$P\bar{1}$	$P\bar{1}$	$P\bar{1}$	$C2/c$	$P\bar{1}$	$P2_1/c$
a/Å	14.144(3)	12.741(2)	7.367(2)	7.531(1)	7.398(1)	9.367(2)	21.135(6)	7.401(1)	10.094(2)
b/Å	14.077(4)	13.120(3)	11.511(5)	11.284(2)	11.006(2)	13.241(2)	17.266(8)	11.485(8)	19.317(4)
c/Å	14.356(3)	16.405(2)	14.179(2)	13.707(4)	14.109(2)	16.189(1)	13.718(3)	14.999(3)	19.372(2)
α/°		104.88(1)	110.19(2)	109.15(2)	108.86(2)	76.58(1)		63.54(2)	
β/°	109.43(1)	97.01(1)	99.26(1)	94.12(2)	95.64(1)	76.56(1)	92.29(2)	76.00(2)	92.23(2)
γ/°		113.61(1)	99.31(2)	102.69(1)	100.31(1)	76.54(2)		80.76(1)	
Z	4	4	2	2	2	2	8	2	4
V/Å^3	2695.90	2348.75	1082.63	1063.60	1054.42	1858.50	4975.84	1106.29	3774.30
μ(Mo-K$_\alpha$)	9.76	11.19	28.97	28.64	30.11	16.46	25.47	23.70	13.48
Unique reflections/ N(reflections used)	4725/3512	8186/4896	3085/3268	3692/2973	3699/2896	5028/3760	4323/2993	3875/3601	6154/4679
R	0.0458	0.0474	0.0693	0.0733	0.0583	0.0323	0.0662	0.0557	0.0444
R'	0.0497	0.0528	0.0693	0.0789	0.0570	0.0361	0.0680	0.0512	0.0482
T/K	298	298	298	298	298	298	298	298	298

stereochemistries of different ML_5 chromophores and to account for these changes in terms of the different bonding roles of the ligands present.[39] The present paper emphasises that, in the special case of the low symmetry CuN_4X chromophore, the vibrational modes of this chromophore alone, can produce the range in stereochemistry of the five-co-ordinate ML_5 chromophore, with the same set of ligands.

Electronic properties of the [Cu(bipy)$_2$Cl][Y] complexes

The polycrystalline electronic reflectance spectra of some representative complexes are shown in Table 3, see refs. 10 and 11 for illustrated examples. The near RTBP complex, **2/3**, involves a broad asymmetric low energy peak at 12000 cm^{-1}, consistent with its τ value of 1.00. The spectrum of **6**, $\tau = 0.79$, shows a broad peak, partially resolved into two peaks, with energies of 11500 and 13500 cm^{-1}, respectively, and appearing to evolve from the single peak at *ca.* 12000 cm^{-1} for a RTBP stereochemistry. Complex **13**, $\tau = 0.62$, which has an intermediate stereochemistry, involves a high energy peak at 14160 cm^{-1}, with a low energy shoulder at 10100 cm^{-1}. The change in peak energy and intensity for the series of eighteen [Cu(bipy)$_2$Cl][Y] complexes, Table 3, can be used to suggest an electronic criterion[40] of the stereochemistries present. A RTBP stereochemistry shows a single peak at ≈12000 cm^{-1}, whereas a SBPDTBP stereochemistry shows two clearly resolved peaks, at ≈10000 and ≈14000 cm^{-1}, respectively.

Experimental

Preparations

All the complexes were prepared from an appropriate copper salt (1 mmol), bipy (2 mmol) and the sodium salt of the appropriate anion, in various aqueous, methanol, acetone or acetonitrile solvent mixtures. Table 4 reports the colour and analytical data of the ten new complexes reported.

Crystallography

The crystallographic and refinement data for the ten new complexes reported are given in Table 5. The unit cell parameters were determined (25 reflections, θ 3–25°) and their intensities collected on an Enraf-Nonius CAD4 diffractometer. Reflections in the range $3.0 < \theta < 24°$ were collected, in one hemisphere or in one quadrant as indicated in Table 5. The data were collected at room temperature using an ω–2θ scan mode, a constant scan speed of 0.05° s^{-1}, with a variable scan width of $(0.8 + 0.2 \tan \theta)$. Lorentz-polarisation corrections were applied, but no correction was made for absorption. Complex atom scattering factors were used for the non-hydrogen atoms.[41] Data reduction was carried out using the program XCAD.[42]

The structures were solved using the SHELX 76[43] and SHELXS 86[44] programs, developed by Fourier difference techniques and refined by full-matrix least-squares analysis. In each case, the least-squares calculations were on $|F|$. Anisotropic thermal parameters were employed for all the non-hydrogen atoms. The positions of the hydrogen atoms were calculated geometrically and "floated" on the appropriate carbon atom positions, assuming C–H distances of 1.08 Å and fixed thermal parameters of 0.07 $Å^2$. The $[CF_3SO_3]^-$ anion of complex **11** involved disorder of the CF_3 fragment as three interpenetrating tetrahedra with a site occupation factor (s.o.f.) of 0.33. The $[NO_3]^-$ anion of **5** involved two interpenetrating NO_3 units with a s.o.f. of 0.5. The $[CF_3SO_3]^-$ anion of **25** was disordered; the CF_3 fragment was refined as a rigid body and the three oxygen atoms were disordered with a s.o.f. of 0.33. The H_2O molecule was disordered over a number of sites.

All calculations were carried out using the SHELX 76,[43] SHELXS 86,[44] XANADU,[45] PUBTAB[46] and XCAD[42] programs on a VAX 6310 computer; PLUTON92[47] was run on a Memorex 386 PC.

The diffuse reflectance spectra in the range 5000 to 30000 cm^{-1} were measured on polycrystalline samples on a Shimadzu UV-VIS 3101 spectrometer.

CCDC reference number 186/1409.

Acknowledgements

The authors acknowledge the award of Forbairt and University College Cork (U.C.C.), Studentships (to G. M., C. O. S. and B. M.), an EOLAS (Irish Science and Technology Agency) grant for the diffractometer, the Computer Bureau, U.C.C., for computing facilities, Professors G. M. Sheldrick and P. McCardle, Drs P. Roberts, S. Motherwell, K. Henrick and A. L. Spek, for the use of their crystallography programs and the Microanalysis Section, U.C.C., for analysis.

References

1 G. Murphy, C. O'Sullivan, B. Murphy and B. Hathaway, *Inorg. Chem.*, 1998, **37**, 240.
2 I. B. Bersuker, *The Jahn-Teller Effect and Vibronic Interactions in Modern Chemistry*, Plenum, New York, 1983.
3 D. Reinen and C. Friebel, *Struct. Bonding* (*Berlin*), 1979, **37**, 1; L. R. Favello, *J. Chem. Soc.*, *Dalton Trans.*, 1997, 4463.
4 I. B. Bersuker, *Coord. Chem. Rev.*, 1975, **14**, 357; J. Gazo, I. B. Bersuker, J. Garaj, M. Kabesova, J. Kohout, H. Langfelderova, M. Melnik, M. Serator and F. Valach, *Coord. Chem. Rev.*, 1976, **19**, 253.
5 H. A. Jahn and E. Teller, *Proc. R. Soc. London*, *Ser. A*, 1937, **161**, 220.
6 J. D. Dunitz, *X-Ray Analysis and the Structure of Organic Molecules*, Cornell University Press, London, 1979, ch. 7.
7 H. Burgi and J. D. Dunitz, *Acc. Chem. Res.*, 1983, **16**, 153.
8 T. Auf der Heyde and H.-B. Burgi, *J. Am. Chem. Soc.*, 1989, **28**, 3960, 3970, 3982; T. Auf der Heyde, *Angew. Chem.*, *Int. Ed. Engl.*, 1994, **33**, 823.
9 B. J. Hathaway, *Comprehensive Coordination Chemistry*, *The Synthesis*, *Reactions*, *Properties and Applications of Coordination Compounds*, eds. G. Wilkinson, R. D. Gillard and J. A. McCleverty, Pergamon, Oxford 1987, vol. 5, pp. 533–774.
10 W. D. Harrison, D. M. Kennedy, N. J. Ray, R. Sheahan and B. J. Hathaway, *J. Chem. Soc.*, *Dalton Trans.*, 1981, 1556.
11 P. Nagle, E. O'Sullivan, B. J. Hathaway and E. Muller, *J. Chem. Soc.*, *Dalton Trans.*, 1990, 3399.
12 S. G. Teoh, H. K. Fun and B. J. Chan, *J. Fizik. Mal.*, 1987, **8**, 44.
13 S. Tyagi, B. J. Hathaway, S. Kramer, H. Stratemeier and D. Reinen, *J. Chem. Soc.*, *Dalton Trans.*, 1984, 2087.
14 F. S. Stephens and P. A. Tucker, *J. Chem. Soc.*, *Dalton Trans.*, 1973, 2293.
15 D. Cunningham, Ph.D. Thesis, National University of Ireland, 1992.
16 W. D. Harrison, B. J. Hathaway and D. M. Kennedy, *Acta Crystallogr.*, *Sect. B*, 1979, **35**, 2301.
17 M. Munakata, L. P. Wu, T. Kuroda-Sowa, M. Yamamoto, M. Maekawa and K. Moriwaki, *Inorg. Chim. Acta*, 1998, **268**, 317.
18 J. Kaiser, G. Brauer, F. A. Schroeder, I. F. Taylor and S. E. Rasmussen, *J. Chem. Soc.*, *Dalton Trans.*, 1974, 1490.
19 S. Bernes, F. Secheresse and Y. Jeannin, *Inorg. Chim. Acta*, 1992, **194**, 105.
20 W. P. Jensen and R. A. Jacobson, *Inorg. Chim. Acta*, 1981, **50**, 189.
21 Q. Minxie, Z. Daoben, L. Mingzhu and Z. Zeying, *Sci. Sin.*, *Ser. B* (*Chinese Ed.*), 1985, 579.
22 M. A. Khan and D. G. Tucker, *Acta Crystallogr.*, *Sect. B*, 1981, **37**, 1409.
23 B. J. Hathaway and A. Murphy, *Acta Crystallogr.*, *Sect. B*, 1980, **36,** 295.
24 G. A. Barclay, B. F. Hoskins and C. H. L. Kennard, *J. Chem. Soc.*, 1963, 5691.
25 A. W. Addison, T. Nageswara Rao, J. Reedijk, J. van Rijn and G. C. Verschoor, *J. Chem. Soc.*, *Dalton Trans.*, 1984, 1349.
26 E. Muller, C. Piguet, G. Bernardelli and A. F. Williams, *Inorg. Chem.*, 1988, **27**, 849.
27 G. Murphy, P. Nagle, B. Murphy and B. J. Hathaway, *J. Chem. Soc.*, *Dalton Trans.*, 1997, 2645.
28 G. Murphy, C. Murphy, B. Murphy and B. Hathaway, *J. Chem. Soc.*, *Dalton Trans.*, 1997, 2653.
29 K. Nakamoto, *Infrared Spectra of Inorganic and Coordination Compounds*, Wiley, New York, 3rd edn., 1978.

30 M. Bacci, *J. Chem. Phys.*, 1986, **104**, 191; R. R. Holmes, R. S. Deiters and J. A. Golen, *Inorg. Chem.*, 1969, **8**, 2612.
31 D. Reinen, *Comments Inorg. Chem.*, 1983, **2**, 227.
32 D. Reinen and M. Atanasov, *Magn. Reson. Rev.*, 1991, **15**, 167.
33 M. Brophy, G. Murphy, C. O'Sullivan, B. Murphy and B. J. Hathaway, *Polyhedron* 1999, **18**, 611.
34 B. J. Hathaway, *Struct. Bonding* (*Berlin*), 1984, **57**, 55.
35 B. J. Hathaway, M. Duggan, A. Murphy, J. Mullane, P. C. Power, A. Walsh and B. Walsh, *Coord. Chem. Rev.*, 1981, **36**, 267.
36 E. L. Muetterties, *Inorg. Chem.*, 1965, **4**, 795.
37 E. L. Muetterties and L. T. Guggenberger, *J. Am. Chem. Soc.*, 1974, **96**, 1748.
38 R. R. Holmes and J. A. Deiters, *J. Am. Chem. Soc.*, 1977, **99**, 3318.
39 J. Pinkas, J. C. Huffman, M. H. Chisholm and K. G. Caulton, *Inorg. Chem.*, 1995, **34**, 5314.
40 B. J. Hathaway, *J. Chem. Soc.*, *Dalton Trans.*, 1972, 1192.
41 D. T. Cromer and J. T. Waber, *International Tables of Crystallography*, Kynoch Press, Birmingham, 1974, vol. IV, pp. 71, 148 (Present distributor Kluwer Academic Publishers, Dordrecht).
42 P. McCardle, XCAD, program for data reduction of CAD4 output, University College Galway, 1990.
43 G. M. Sheldrick, SHELX 76, program for crystal structure determination, University of Cambridge, 1976.
44 G. M. Sheldrick, SHELXS 86, program for crystal structure solutions, University of Göttingen, 1986.
45 P. Roberts and G. M. Sheldrick, XANADU, program for the calculation of crystallographic data, University of Cambridge, 1979.
46 K. Henrick, PUBTAB, program to prepare and print crystallographic tables for publication, University of North London, 1980.
47 A. L. Spek, PLUTON92, program for the illustration of molecular structures, University of Utrecht, 1992; *Acta Crystallogr.*, *Sect. A*, 1990, **46**, C-34.

Paper 8/10020I